Preparation of Multilayered Trimodal Colloid Crystals and Binary Inverse Opals
Supporting Information

Jianjun Wang, Qin Li, Wolfgang Knoll, Ulrich Jonas*

Max Planck Institute for Polymer Research, Ackermannweg 10, 55128 Mainz, Germany; contact: Tel.: +49 6131 379 163, Fax: +49 6131 379 100, jonas@mpip-mainz.mpg.de

Experimental:

Monodispersed polystyrene particles used in the experiments were prepared by surfactant-free emulsion polymerization[1] and were purified by several circles of centrifugation and re-dispersion in ultrapure water (Milli-Q system from Millipore GmbH, Eschborn, Germany). PMMA particles were prepared by emulsion polymeriztion[2] and washed with copious of Milli-Q water by filtration through a solvent resistant stirred cell XFUF 07601 (Millipore GmbH). A low –voltage scanning electron microscope (LV-SEM, LEO Gemini 1530) was used to measure polymer particle sizes by taking the average of at least 200 particles. The LV-SEM images were taken on native samples (non-sputtered) at acceleration voltages of 0.2-1 kV. The particle size determined by SEM is 2-4% smaller than that measured by dynamic light scattering, DLS (Zeta Sizer 3000HS, Malvern Instrument Ltd.), which is due to hydration of the hydrophilic particle shell, increasing the hydrodynamic radius in suspension (relevant for DLS). Silica nanoparticles used in the experiments were obtained from EKA Chemicals. Vis-NIR spectra were taken with a Lambda UV/VIS/NIR- & UV/VIS Spectrometer (Perkin-Elmer).

Glass substrates, cleaned by immersion into piranha solution (H_2O_2 : H_2SO_4=30:70, v/v. *Caution: piranha solution reacts violently with organic compounds*

and must be handled with extreme care !) and washed by copious amounts of ultrapure water, were lifted from the colloidal suspensions by a home made dipping devise. The typical lifting speed was 12 μm / min.

The total film thickness of the colloidal films prepared by vertical lifting deposition depends, as in the case of monomodal and bimodal colloidal crystals,[8,9] on the particle concentration in suspension and on the substrate lifting velocity, with higher concentrations and lower lifting velocities leading to thicker layers. By adjusting these parameters, in our lab we have prepared different composite colloidal crystal films consisting of a single large particle layer up to a total thickness of 14 large particle layers.

The described procedure to form composite colloidal crystals is applicable to a large range of particle sizes and materials. For example, binary colloidal crystals were successfully prepared from combinations of large and intermediate polymer particles with diameters of 330/52, 362/95, 476/87, 489/95, 520/129, 839/187, 839/205 and 978/135 (nm/nm). For inverse opals with polymer particles as sacrificial templates and nanoparticles as structure forming materials, silica nanoparticles with sizes of either 6nm or 10nm, CdSe quantum dots (3nm diameter, coated with thioglycolic acid), and CdSe/ZnS alloy nanoparticles (3nm diameter, coated with thioglycolic acid) could all be used as the matrix material and PS particles of size large than 125 nm as the templates. In related work by other authors binary colloidal crystals and corresponding inverse opals could be prepared with TiO_2 and gold nanoparticles.[10,11]

Defects Analysis:

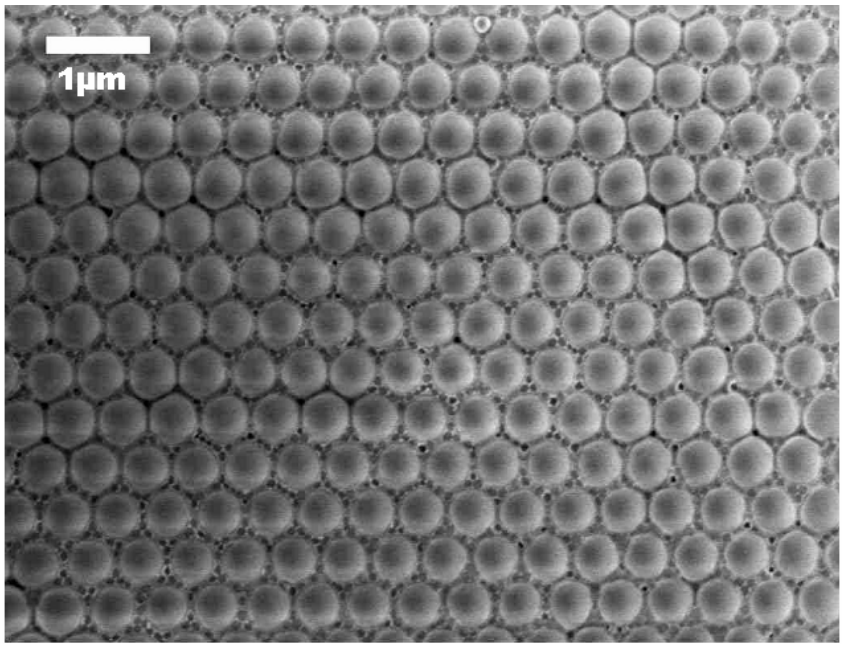

Fig. S1a: SEM of trimodal colloidal crystal with PS microspheres of a diameter D = 465 nm as the large particles, PMMA nanospheres D = 84 nm as the intermediate colloids, and silica nanoparticles D = 6 nm as the small component. The relative size ratios were $\gamma_{I/L} = D_{Intermediate} / D_{Large} = 0.18$, and $\gamma_{S/I} = D_{Small} / D_{Intermediate} = 0.071$, while the relative concentrations were $\phi_{I/L} = C_{Intermediate} / C_{Large} = 0.09$ and $\phi_{S/I} = C_{Small} / C_{Intermediate} = 1.1$ with the total volume fraction of PS particles being $\phi_{PS} = 0.01$.

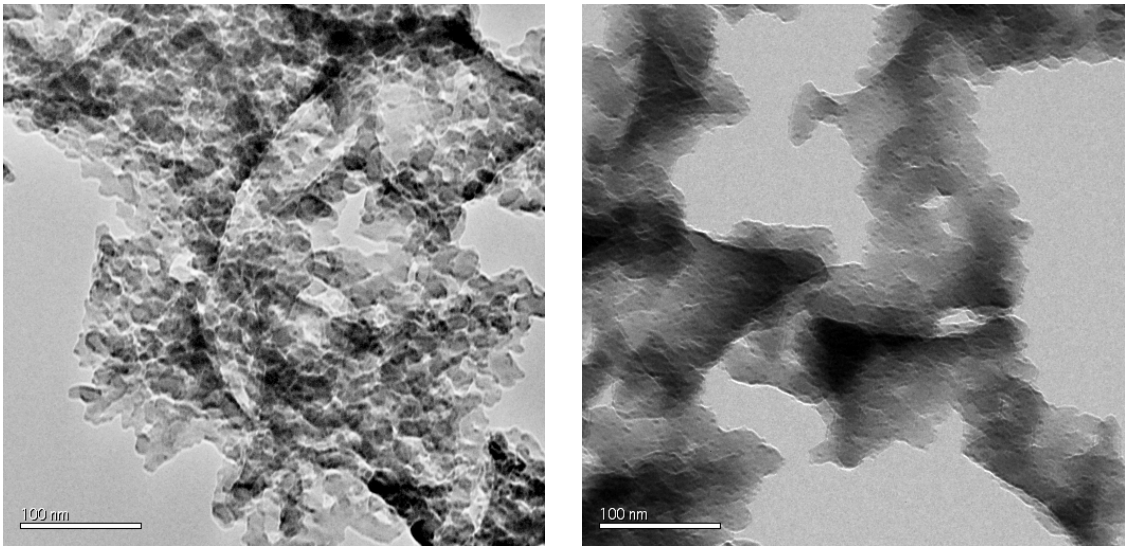

Fig. S1b: TEM images of the SiO_2 matrix (here from a mIO) show a granular morphology, which explains the lower refractive index compared to bulk silica.

The typical defects that exist in the monomodal colloidal crystals (mCC, crystals consisting of only one colloidal component) formed by vertical deposition, such as point defects (e.g. vacancies), line defects (e.g. dislocations), planar defects (e.g. stacking faults), and cracks, were also found in our tCC structures and well identified in the SEM images. In the present mCCs the approximate diameter of compact domains between cracks were in the order of 10-50 µm, an approximate point defect areal density was about 0.005 μm^{-2} at the crystal surface, while line defects and stacking faults were found about every 5-10 µm. Additional defects of the tCCs (analogous to bCCs) are visible in Figure S1, which shows a single domain between cracks (usually regions of several tens to several hundreds large PS particles in diameter). These additional defects result mainly from the packing disorder of the intermediate PMMA particles and can be considered as "stoichometric" defects as a variation of the number ratio of intermediate and large

particles without affecting the high hexagonal order of the large particles. By analysis of the SEM images a stoichiometric surface defect density of 16% was found in the tCC.

A further origin of defects may result from a particle shape asymmetry, as it can be observed for the larger PS particles in the SEM images (e.g. in Figure 1). This shape distribution is inherent to the particle preparation process, but it does not interfere with their ability to form highly ordered colloid crystals.

Spectra Analysis:

Since in our experiments the incident light enters the fcc (111) plane of the colloidal crystals and inverse opals in the normal direction, the stop band positions can be approximated by Bragg's law as:[3]

$$\lambda = (8/3)^{1/2} d n_{avg} \quad (1)$$

where λ is the wavelength of the stop band maximum, d is the scattering lattice periodicity which coincides with the diameter of the large PS sphere, n_{avg} is the average refractive index of the material, which can be derived by:[3]

$$n^2_{avg} = \sum_i n^2_i \phi_i \quad (2)$$

where n_i and ϕ_i are the refractive index and volume fraction of each component i in the film. In other words, once we know the n_i and ϕ_i for each component of the crystal material, we are able to obtain a theoretical stop band maximum by Eqs. (1) and (2). Since the PS volume fraction and the refractive indices for the PS and PMMA particles and air are known, the volume fraction for the PMMA particles and the refractive index for the silica nanoparticle matrix remain to be calculated.

Firstly, the spectral data of a mCC made from large PS particles was used to test the consistency between the theoretical values and experimental measurements for our systems. The stop band maximum of the mCC(PS/air) with fcc lattice geometry can be calculated by assuming ϕ_{PS} of 0.74 (n_{PS}=1.59) and ϕ_{air} of 0.26 (n_{air}=1), resulting in λ = 1108 nm, which is about 1 % lower than the measured wavelength of 1122 nm. Thus, a ±1% deviation can be considered as the system error.

Secondly, we considered the bCC(PS/PMMA/air) to derive a value for the filling fraction of the PMMA particles. In the case of bCC(PS/PMMA/air), which comprises large (L) PS particles and intermediate (I) PMMA particles (n_{PMMA} = 1.49) with air filling the voids, the large PS particles remain in a fcc lattice structure, i.e., ϕ_{PS} of 0.74. Using Eqs. (1), (2), and the measured maximum stop band wavelength of 1138 nm (taking into account the 1% system error) we calculated the PMMA volume fraction, ϕ_{PMMA}, in the bCC as 9 ± 3% (nevertheless, a wavelength of 1138 nm would correspond to an exact value of ϕ_{PMMA} = 9.4%).

Thirdly, the refractive index of the silica nanoparticle matrix was obtained as follows. When 6 nm silica nanoparticles were added to the suspension mixture to prepare the tCCs, the silica nanoparticles occupied in the particle deposition process the free volume among the PS and PMMA spheres in the manner of random closed packing (RCP), without obstructing their binary packing structures or changing the PS/PMMA stoichiometry going from the bCC to the tCC (as indicated by SEM data). To avoid the controversy about RCP density[4] as well as the *exact* refractive index of the silica

nanoparticles, we treated the silica nanoparticle matrix as a amorphous medium and attributed an effective refractive index to this matrix, $n_{SilicaMatrix}$. Its value was deduced from the stop band wavelength of the monomodal inverse opal (mIO) using Eqs. (1) and (2), with ϕ_{air} = 0.74, and $\phi_{SilicaMatrix}$ = 0.26. When treating the mIO data (stop band maximum wavelength = 776 nm), a 3% shrinkage of the lattice constant due to the pyrolysis was taken into account in the calculation. The refractive index $n_{SilicaMatrix}$ was derived as 1.19, which is significantly lower than the refractive index of silica bulk material ($n_{SilicaBulk}$ = 1.43), mainly due to two factors: a.) the silica-air matrix contains a considerable amount of air volume; b.) the properties of nanoparticles (including refractive index) are known to potentially differ from that of their bulk materials.[5,6]

Using $n_{SilicaMatrix}$ = 1.19, ϕ_{PMMA} = 9.4%, and ϕ_{PS} = 0.74, the stop band wavelength for tCC was calculated with Eqs. (1) and (2) as 1156 nm, which is extremely close to the measured spectra maximum of 1158 nm. This confirms the validity of the values calculated for $n_{SilicaMatrix}$ as well as for ϕ_{PMMA}, and the assumption, that the refractive index of the silica matrix is essentially the same *before* and *after* pyrolysis.

The spectral data of the binary inverse opal bIO(silica/air) was also used to confirm the volume fraction of the intermediate PMMA particles. When we substituted ϕ_{air} as the summation of the original ϕ_{PMMA} and ϕ_{PS}, i.e, 83.4%, and $n_{SilicaMatrix}$ = 1.19, considering the 3% shrinkage in the lattice constant, the stop band wavelength was calculated as 762

nm, which is within 1% deviation from the measured wavelength (755nm). This further corroborates the legitimacy of the values determined for ϕ_{PMMA} and $n_{SilicaMatrix}$.

Given the size ratio of $\gamma_{I/L}=D_{Intermediate}/D_{Large}=0.18$, the value of ϕ_{PMMA} can be further translated into the crystal structure in the formed bCC and tCC, and the pore architecture in the bIO. The deduction shows that each large PS sphere is coordinated by about 21-23 intermediate PMMA particles, i.e. $LI_{21\text{-}23}$ in terms of stoichiometry.

Computer Models:

A geometrical analysis and computer modelling was conducted to determine the maximum number of intermediate particles ($\gamma_{I/L}=D_{Intermediate}/D_{Large}=0.18$) that can be fitted into the interstitial tetrahedral and octahedral sites in a face-centred cubic (fcc) lattice of large spheres. The motivations are twofold: firstly, it is to provide the quantitative description of the packing geometry of the intermediate particles; secondly it is to validate the stoichiometric ratio obtained from the spectroscopically derived PMMA volume fraction. A comprehensive phase diagram including multiple binary colloidal crystal structures was provided by Hynninen et al.[7] for oppositely charged particles with a size ratio of 0.31. These bCCs were formed under thermodynamic equilibrium conditions in suspension. In their phase diagrams the stoichiometry of LI_{23}, as found in our experiments, is not present. It is important to note that in our experiments the PS and PMMA colloids were both negatively charged, the particle size ratio was 0.18, and the bCC was formed under non-equilibrium conditions during vertical transfer. Therefore, this bCC structure does not fall in the regime predicted by these authors.

In the present computer models, the particles are considered as hard spheres, and a set of criteria were applied in searching for the optimal positions for the intermediate particles:

1. No particles are allowed to overlap with any other particles.
2. Each particle must be in touch with at least one other particle.
3. The first intermediate particle entering the void must occupy the most stable position (i.e., in the threefold hollow site between 3 big particles).
4. The intermediate particles occupy the voids in a trigonal-symmetrical manner.

In general, the optimum packing position is searched by assigning a guessed initial position, and a moving direction. The particle in question keeps on moving till maximum contact points are reached.

The computer assisted analysis shows that for the given size ratio of 0.18, a tetrahedral site, formed by 4 large particles, accommodates at most 4 such intermediate particles, and that an octahedral site formed by 6 large particles accommodates at most 15 such smaller particles. Since each large particle is surrounded by 6 octahedral sites and 8 tetrahedral sites, the stoichiometry structure resulted in LI_{23}. This matches extremely well with the volume fractions and $LI_{21\text{-}23}$ stoichiometry deduced from the spectroscopic data, particularly considering the inevitable experimental errors involved.

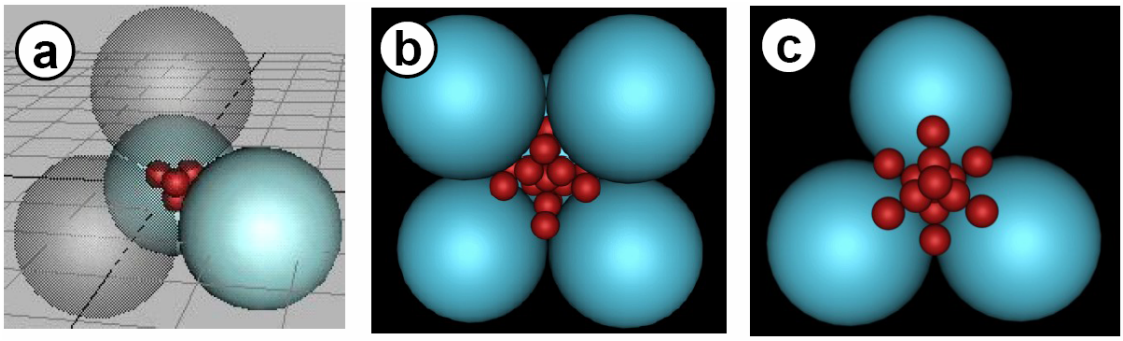

Figure S2: Additional images of the computer models for the tetrahedral and octahedral sites formed by large spheres with voids filled by intermediate particles ($\gamma_{I/L}$= 0.18). a) tetrahedral site with 2 large particles set as transparent; b) a rotated side view of the octahedral site with one large sphere (on top) removed; c) top view of the octahedral site with 3 large spheres at the top removed.

[1] G. T. D. Shouldice, G.A. Vandezande, A. Rudin, *Eur. Polym. J.* **1994**, *30*, 179-183.

[2] U. Jonas, C. Krüger, *J. Supramol. Chem.* **2002**, *2*, 255-270.

[3] H. Miguez, C. Lopez, F. Meseguer, A. Blanco, L. Vazquez, R. Mayoral, M. Ocana, V. Fornes, A. Mifsud, *Appl. Phys. Lett.* **1997**, *71*, 1148-1150.

[4] A. Donev, F. H. Stillinger, S. Torquato, *Phys. Rev. Lett.* **2006**, *96*, 225502-1-4

[5] R. Tsu, D. Babic, L. Ioriatti Jr., *J. Appl. Phys.* **1997**, *82*, 1327-1329

[6] C. R. Snyder, J. F. Douglas, *J. Phys. Chem. B* **2000**, *104*, 11058-1165.

[7] A.-P. Hynninen, C. G. Christova, R. van Roij, A. van Blaaderen, M. Dijkstra, *Phys. Rev. Lett.* **2006**, *96*, 138308-1-4

[8] Charles-André Fustin, Gunnar Glasser, Hans W. Spiess, Ulrich Jonas, *Langmuir* **2004**, *20*, 9114-9123.

[9] Wang, J.; Glasser, G.; Neumann, T.; Burkert, K.; Li, Q.; Knoll, W.; Jonas, U. submitted to *Adv. Mater.* **2006.**

[10] Q.-B. Mang, C.H. Fu, Y. Einaga, Z.-Z. Gu, A. Fujishima, O. Sato, *Chem. Mater.* **2002**, *14*, 83-88

[11] P. M. Tessier, O. D. Velev, A. T. Kalambur, A. M. Lenhoff, J. F. Rabolt, E. W. Kaler, *Adv. Mater.* **2001**, *13*, 396-400